The reverse-DADI method: Computation of frequency-dependent atomic polarizabilities for carbon and hydrogen atoms in hydrocarbon structures

Sylvain Picaud, Michel Devel, Faoulat Miradji, Nicolas Brosseau-Habert

Journal of Quantitative Spectroscopy & Radiative Transfer 329 (2024) 109194

Contents lists available at ScienceDirect

Journal of Quantitative Spectroscopy and Radiative Transfer

journal homepage: www.elsevier.com/locate/jqsrt

The reverse-DADI method: Computation of frequency-dependent atomic polarizabilities for carbon and hydrogen atoms in hydrocarbon structures

N. Brosseau-Habert [a,b], F. Miradji [a], S. Picaud [b,*], M. Devel [a]

[a] Institut FEMTO-ST – UMR 6274 SUPMICROTECH/Université de Franche-Comté/CNRS, Besançon, France
[b] Institut UTINAM - UMR 6213 Université de Franche-Comté/CNRS, Besançon, France

ARTICLE INFO

Keywords:
Atomic polarizability
Hydrocarbons
Absorption cross section
Computational method
Astrophysics

ABSTRACT

A specific method, combining some ingredients of the well-known DDA and PDI approaches, has been developed in our group since many years to calculate the absorption cross-sections of carbonaceous nanoparticles based on their atomistic details. This method, here named the Dynamic Atomic Dipole Interaction (DADI) model, requires the knowledge of the position and frequency-dependent polarizability of each atom constituting the nanoparticles. While the atomic positions can be quite easily obtained, for example as the results of molecular dynamics simulations, obtaining the frequency-dependent atomic polarizabilities is a trickier task. Here, a fitting procedure, named the reverse-DADI method, has been applied to calculate the frequency-dependent atomic polarizability values for carbon and hydrogen atoms involved in aromatic cycles or in aliphatic chains, on the basis of frequency-dependent molecular polarizabilities of various PAH and alkane molecules, calculated with the TD-DFT theory, in the UV–Visible range. Then, using these frequency-dependent atomic polarizabilities as input parameters in the DADI model has been shown to lead to an accurate representation of the absorption cross-sections of various PAH and alkane molecules with respect to the corresponding values obtained at the TD-DFT level, with however the great advantage of a much shorter time of calculations. Furthermore, these results are indications of a good transferability of the frequency-dependent atomic polarizability values obtained here to any C or H atom of any PAH or alkane molecule. This opens the way for building large databases of optical properties for carbonaceous species of atmospheric or astrophysical interests.

1. Introduction

Massive amounts of carbonaceous matter, originating from incomplete combustion of fossil fuel and biomass burning, are emitted into the atmosphere every year, mainly in the form of black carbon (BC) aerosols [1]. These aerosols are suspected to have a significant impact on radiation forcing of Earth's atmosphere, thus contributing to climate warming [2–5]. BC aerosols may also impact on the quality of ambient air [6], making their emissions a public health concern [7,8]. However, quantifying the influence on climate and on health of BC aerosols remains challenging, and numerous research projects are still devoted to elucidate the physico-chemical characteristics and properties of the corresponding nanoparticles, as well as their ageing processes. From the climate point of view, not only BC particles directly interact with incoming solar radiation (absorption/diffusion processes) driving their direct impact on radiative forcing [9], but they also interact with the surrounding water molecules to act, more or less efficiently, as cloud condensation nuclei. This may then lead to the subsequent formation of clouds [10], which influence themselves the climate (BC thus contributes to what is usually called the indirect effects of atmospheric particles) [4]. Besides, the impact on health and environment is certainly closely related to the ability of these particles to carry harmful chemical compounds such as polycyclic aromatic hydrocarbons (PAHs) or heavy metals [11,12]. Thus, a thorough understanding of the behavior of BC nanoparticles requires as precise as possible knowledge of, e.g., their morphology, their surface chemistry and their interactions with the surrounding atmospheric species and, more generally, a better characterization of their sources and scavenging processes.

It is worth noting that combustion particles are essentially made of carbon aggregates [13–15], the units of which having certain similarities with various forms of carbonaceous material observed in the interstellar medium (ISM) [16,17] and also likely present in the atmospheres of exoplanets [18–21].

Indeed, astronomical observations highlight broad infrared emission features called "Aromatic Infrared Bands" (AIBs) [22–24], as well as "Diffuse Interstellar Bands" (DIBs), representing more than 300 absorption features observed in the near-UV, visible and near-infrared ranges

* Corresponding author.
E-mail addresses: sylvain.picaud@univ-fcomte.fr (S. Picaud), michel.devel@femto-st.fr (M. Devel).

https://doi.org/10.1016/j.jqsrt.2024.109194
Received 22 May 2024; Received in revised form 10 September 2024; Accepted 11 September 2024
Available online 13 September 2024

along interstellar sightlines reddened by interstellar dust [25,26]. The observations also reveal a broad ultraviolet absorption bump on the ISM extinction curve from the Milky Way to high-redshift galaxies, with a stable position centered at 217.5 nm [27–29]. The presence of molecular structures containing numerous carbon–carbon and carbon–hydrogen bonds appears as a natural interpretation of these data [30], thus suggesting complex carbon chemistry at work, involving large carbonaceous species, ranging from tens to thousands of atoms, on the boundary between big molecules (such as PAHs, fullerene, slabs of graphite, etc.) and solid grains [31–34].

Thus, in addition to being mainly made of carbon atoms, carbonaceous interstellar particles and BC aerosols have in common the need for a better characterization of their interaction with radiation in the UV–Visible-IR range, aiming at usefully interpret the results of remote sensing observations from Earth or satellites, and also their climate impact, in the case of BC. Moreover, it is also worth noting that observations of the interaction of these various carbonaceous particles with light is the only way to characterize their structure in situ, as the optical properties of the nanoparticles themselves may strongly depend on their morphology [35,36].

From a theoretical point of view, absorption and scattering properties can be computed analytically for particles whose dielectric constant or refractive index is known [37]. Thus, by assuming the shape, the size and even the internal composition (i.e., the organic carbon over total carbon - OC/TC - ratio) of the particles, the Lorenz–Mie theory and/or the Rayleigh–Debye–Gans theory can reproduce quite well the measured optical properties of combustion-emitted particles [38–40]. Moreover, powerful numerical approaches such as the T-matrix [41–43] or the Discrete Dipole Approximation (DDA) [44–48] methods are now largely used for quantifying absorption and scattering of radiation by particles of arbitrary shape and by periodic structures (see, for instance, the recent review on these modeling approaches by Kahnert and Kanngießer [35]). Nevertheless, the underlying assumptions of all these methods usually prevent considering the atomistic details of the carbonaceous particles, such as the presence of numerous structural point defects at their surface, [49] or the local changes of atomic hybridization due to overlapping and necking phenomena observed when these particles form aggregates [50,51]. These features have, however, been proven to have a non-negligible impact on the optical properties of the particles [52–55], and, as a consequence, they should not be ignored, whether we are interested in a better quantification of the radiative forcing due to combustion-generated particles, or in the identification of interplanetary dust, on which, in addition, organic compounds can be adsorbed [56–58].

Another way for characterizing the optical properties which accounts for the atomistic details of the system under consideration is the point dipole interaction (PDI) method (initially called Atom Dipole Interaction (ADI) method) [59,60], in which the molecular polarizability is obtained from solving linear equations for a set of atomic polarizabilities, coupled all together due to the interaction of each induced atomic dipole moment with both the external electric field and the electric field due to the other induced atomic dipole moments. Once extended to incorporate possible charge transfers between atoms, this PDI model has been extensively used for the calculations of polarizabilities of various carbonaceous systems such as large aliphatic and aromatic molecules [61–63], fullerenes [63–66], carbon nanotubes [66–68], olephinic molecules [69], and even large molecular clusters formed by linear chains of up to 300 urea molecules and one- and two-dimensional clusters of C_{60} with up to 25 molecules [70]. The PDI method has also been extended to the case of complex frequency-dependent atom polarizabilities allowing the computation of, e.g., absorption cross-sections. This has been first done by using simple models such as a distribution of oscillators with Lorentzian band-shape on each atom of the investigated systems [71,72] and, later, by considering more sophisticated descriptions based on frequency-dependent quasi-static interaction models with electric charge transfer between atoms and atom dipole moments (the so-called CT-PDI model) [73–75]. Note that these calculations used the non-retarded form of the interaction tensors to compute the electric field created by an electric dipole or an effective charge. Hence the parametrizations obtained or used in those papers cannot be safely used with the retarded interaction tensor of vacuum used in DDA. Since our mid-term goal is to compute optical properties of soot grains with a least one characteristic length of the order of the characteristic wavelength of the incoming wave, it is necessary to obtain new parametrized atomic polarizabilities compatible with the retarded interaction tensor. Besides, our long-term goal being the creation of large databases of optical properties to help at interpreting visible-UV measurements, it is necessary to have environment-dependent parametrizations of the atomic polarizabilities to take correctly into account subtle differences that might be used for the experimental differentiation between various chemical functions. In this context, we have developed in Besançon a numerical method aiming at computing optical properties of soot nanoparticles, that directly depends on their atomistic details, i.e., all the atomic positions and the frequency-dependent polarizabilities of each type of atoms constituting the particles [76,77]. This atomistic approach is directly inspired by both DDA and PDI methods, because it uses classical equations of DDA, but directly works with the cartesian coordinates and the frequency-dependent polarizability tensor of each atom, as in PDI, instead of using positions defined on a discretized cartesian grid and effective polarizabilities calculated from macroscopic dielectric permittivity, as in DDA. This method has proven to be suitable for calculating the mass absorption coefficient of elementary carbon nanoparticles modeled at the atomic scale [78,79]. To be more explicit, this method simply named the *PDI-like method* in a previous paper [79] will here be referenced as the Dynamic Atomic Dipole Interaction (DADI) model.

While the atomic positions can be modeled in a sufficiently realistic way from the increasingly accurate results coming from experiments such as, for instance, high-resolution electron microscopy studies [49, 80–82], obtaining precise values of frequency-dependent atomic polarizabilities is a much trickier task, especially because the value of the polarizability is likely to change not only with the type of the atoms but also with their hybridization. In our previous works, we made use of atomic polarizability values either coming from available experimental data obtained on graphite [76–78], or directly fitted on the results of quantum calculations performed on fullerene molecules, to mimick also curvature effects [79]. However, graphitic-like or fullerenic-like carbon atoms cannot be fully representative of the diversity of carbon atom types present in real soot nanoparticles nor in carbonaceous grains of the ISM. It is indeed now clearly established that carbonaceous grains contain not only aromatic but also aliphatic carbons as well as carbon atoms with fewer than 3 neighbors when they are located, e.g., at the edges or at defective sites of the nanoparticles [49,83–85]. Of course, these grains may also contain hydrogen atoms attached to the carbons.

Thus, to complement our previous studies, here we have computed the frequency-dependent atomic polarizabilities for carbon and hydrogen atoms, depending on their vicinity, in PAH and aliphatic molecules. This has been done by using a fitting procedure similar to that previously used when considering fullerene [79], but based here on the frequency-dependent molecular polarizabilities of a set of PAHs and alkanes computed with the time dependent density functional theory (TD-DFT) method [86]. Then, the frequency-dependent atomic polarizabilities resulting from the various fits have been used to calculate, with the DADI method, absorption cross sections for molecules of, e.g., astrophysical interest that were not initially included in the fitting procedure. The comparison of the resulting values with those obtained from TD-DFT calculations performed on the same molecules has then been used as a benchmark of the transferability of the frequency-dependent atomic polarizability of the carbon and hydrogen atoms coming from the fits.

In Section 2, we briefly recall the details of the DADI model that has been used to compute optical properties from atomistic information. In

this Section, we also give the principles of the reverse-DADI method, that has allowed the computation of frequency-dependent atomic polarizabilities from fitting the results of TD-DFT calculations. In Section 3, we describe the computational method used to get the frequency-dependent molecular polarizabilities of various aromatic and aliphatic molecules with TD-DFT calculations. The results of the reverse-DADI method are then given in Section 4, together with the absorption cross sections calculated by the DADI model when using the fitted frequency-dependent atomic polarizabilities. Finally, the main conclusions of this study are summarized and future developments are outlined in Section 5.

2. The DADI model and the reverse-DADI method

2.1. The DADI model

Due to the very large number of electrons to be taken into account, an *ab initio* study based on the direct resolution of the many-electron Schrödinger equation would currently have prohibitive computational cost to get accurate values of the optical properties of carbonaceous grains made of thousands of atoms. This is why the DADI parametrized semi-empirical model has been developed and successively improved in Besançon for many years [76–79]. The main ingredients of this DADI model are briefly recalled below. Thus, by considering $\vec{r}_i$ the position of the atom i and ω the excitation circular frequency, the dipole $\vec{p}_i(\omega)$ induced by the local electric field $\vec{E}_{loc}(\vec{r}_i,\omega)$ at the location of the atom i can be computed by solving the following equations, for i running from 1 to N, the total number of atoms in the particle under investigation:

$$\vec{p}_i(\omega) = \bar{\bar{\alpha}}_i(\omega)\vec{E}_{loc}(\vec{r}_i,\omega) \tag{1}$$

where $\bar{\bar{\alpha}}_i(\omega)$ is the frequency-dependent atomic polarizability tensor of atom i.

Taking into account that the local field $\vec{E}_{loc}(\vec{r}_i,\omega)$ is the sum of the incident field $\vec{E}_0(\vec{r}_i,\omega)$ applied to the particle and of the electric field created at the position $\vec{r}_i$ ($\forall i = 1,\ldots,N$) by the dipoles induced on all the other atoms, Eq. (1) can be rewritten as

$$\vec{p}_i(\omega) = \bar{\bar{\alpha}}_i(\omega)\vec{E}_0(\vec{r}_i,\omega) + \sum_{j=1}^{N} \bar{\bar{\alpha}}_i(\omega)\bar{\bar{T}}(\vec{r}_i,\vec{r}_j,\omega)\vec{p}_j(\omega) \tag{2}$$

where $\bar{\bar{T}}$ can be computed with the double gradient of the generalized vacuum Green's function for the Helmholtz equation as

$$\bar{\bar{T}}(\vec{r}_i,\vec{r}_{j\neq i},\omega) = -\frac{1}{\epsilon_0}(\nabla_{\vec{r}_i}\otimes\nabla_{\vec{r}_j} + \frac{\omega^2}{c^2}\bar{\bar{I}})(-\frac{e^{i\frac{\omega}{c}|\vec{r}_i-\vec{r}_j|}}{4\pi \mid \vec{r}_i-\vec{r}_j \mid}) \tag{3}$$

with c the speed of light, ϵ_0 the vacuum permittivity and $\bar{\bar{I}}$ the identity tensor.

Because in the DADI model the point dipoles are in fact atoms, that is they are much smaller than the discretization volumes used in the DDA [44,45], the $i = j$ terms of the interaction tensor $\bar{\bar{T}}$ are assumed to simplify as

$$\bar{\bar{T}}(\vec{r}_i,\vec{r}_i,\omega) = i\frac{2}{3}\frac{\omega^3}{c^3}\frac{1}{4\pi\epsilon_0}\bar{\bar{I}}. \tag{4}$$

Eq. (2) is thus a $3N\times 3N$ matrix system whose resolution gives a $3\times 3N$ vector containing the dipoles $\vec{p}_i(\omega)$ on each carbon atom, corresponding to three values of $\vec{E}_0$ successively applied along the three (cartesian) coordinate axes. Once the values of the dipoles are self-consistently computed, they can be used to calculate various optical quantities of interest, such as the Mueller matrix, or the extinction, diffusion and absorption cross sections, as in DDA [44,45].

2.2. The reverse-DADI method

In the DADI model, the knowledge of frequency-dependent atomic polarizabilities $\bar{\bar{\alpha}}_i(\omega)$ for each atom type is needed to compute the molecular polarizability tensor $\bar{\bar{\alpha}}(\omega)$ and the optical properties of the system under consideration [79]. Because we aim at characterizing optical properties of carbonaceous grains, possibly coated with PAHs, it is necessary to have relevant values of the frequency-dependent atomic polarizabilities of carbon (with various degrees of hybridizations) and of hydrogen atoms. Therefore, in our previous studies [76–78], carbon anisotropic atomic polarizabilities computed from the graphite dielectric constant tabulated by Draine [87–89] together with the generalized Clausius–Mossotti relation proposed by Senet et al. [90] have been used to calculate the molecular polarizability tensor of various carbonaceous nanoparticles modeling nascent soot. More recently, data coming from fullerenic systems have also been introduced in our approach, to take into account curvature effects of the soot structure [79].

Here, thanks to an improved version of the home-made Python code used in Ref. [79], anisotropic frequency-dependent atomic polarizability of carbon sp^2, isotropic frequency-dependent atomic polarizability of carbon sp^3 and isotropic frequency-dependent atomic polarizability of hydrogen have been fitted on the frequency-dependent molecular polarizabilities of a set of PAH and alkane molecules, obtained by performing TD-DFT calculations. This fitting procedure has thus been called *the reverse-DADI method*, because it aims to fit the atomic polarizabilities from molecular spectra, while the DADI model uses atomic polarizabilities to find optical spectra of molecules and molecular aggregates. Indeed, fits have been achieved by finding the best set of frequency-dependent atomic polarizabilities that, when used as input in the DADI model, have given in turn the best match between the frequency-dependent molecular polarizabilities of the dataset and the ones computed with the DADI model. Because frequency-dependent atomic and molecular polarizabilities are complex numbers, it is worth mentioning that being able to fit the real and imaginary parts of frequency-dependent atomic polarizabilities of one atom type, requires at least one frequency-dependent complex molecular polarizability tensors (together with the file containing the corresponding atomic coordinates). Hence, our fitting procedure has been based on the least-square method which is used to minimize the square of the modulus of the differences between molecular polarizabilities computed at the TD-DFT level and those computed by the DADI model as a function of the fitted atomic polarizabilities, in a given energy range. This procedure is similar to that developed by Jensen et al. [62,70] who also used quantum chemical calculations of molecular polarizabilities for the parametrization of atomic or bond polarizabilities on the basis of a trial set of molecules, in the framework of the dipole interaction model. In addition, note that the least-square procedure we used has been coupled to the L-BFGS-B (Limited Broyden–Fletcher–Goldfarb–Shanno) minimization method to ensure the convergence of the fitted parameters. The truncated Newton conjugate algorithm has also been tested, without however significant improvements.

3. Computation of UV–visible absorption cross sections and of frequency-dependent molecular polarizabilities with TD-DFT

3.1. Principles of the method

To get the values of the frequency-dependent molecular polarizabilities that are requested in the fitting procedure of the reverse-DADI method described above, we have made use of the density functional theory and its time-dependent extension (TD-DFT) [86], as implemented in the Octopus code [91,92], which is a method of choice for the study of the excited-state properties of large molecules such as PAHs or alkanes. Indeed, a large enough number of such molecular species has been needed to supply the database of frequency-dependent molecular polarizability values that are required in the fitting procedure of

the frequency-dependent atomic polarizability of carbon and hydrogen atoms.

The calculation of the real and imaginary parts of these frequency-dependent molecular polarizabilities is divided in three steps [86,91,92]. First, Octopus performs a calculation of the electronic wave functions of a given molecule in its ground state. The Kohn–Sham method of DFT, on which Octopus is based, assumes that, for each interacting ground-state density $\eta(r)$, a non-interacting electron system exists with the same ground-state density. The non-interacting ground state is thus obtainable through the solution of the Kohn–Sham equations. Because of the functional dependence on the density, these equations form a set of nonlinear coupled equations, and the standard procedure to solve them is iterated until self-consistency is achieved.

The second step aims to carry out the time-propagation of the ground-state electronic orbitals when the molecule is subjected to electromagnetic excitation: this is the "time-dependent" calculation. For simulating the excitation of the molecule by an electromagnetic wave, the scheme proposed by Yabana and Bertsch [93] is used, exciting all frequencies of the system by giving a small momentum K to the electrons, thus transforming the wave functions computed in the ground-state. Then, Octopus proceeds to the time-propagation of these wave functions. The result of this calculation, which must be done independently for the 3 cartesian directions of the incident perturbation, is stored in 3 files (one per direction) containing the values of the dipolar moments of the system in the 3 directions of cartesian space, for all the excitation frequencies considered.

Note that, to get the real and imaginary parts of the frequency-dependent molecular polarizability for a given molecule, we have first directly computed the real and imaginary parts of the cross sections σ using the utility of Octopus called *oct-propagation_spectrum*. Thus, two tensors have been calculated, that are directly related to the real and imaginary parts of the molecular polarizability as

$$\sigma_{ij}^{\mathrm{Im}}(\omega) = \frac{4\pi\omega}{c}\,\mathrm{Im}(\alpha_{ij}(\omega)), \tag{5}$$

and

$$\sigma_{ij}^{\mathrm{Re}}(\omega) = \frac{4\pi\omega}{c}\,\mathrm{Re}(\alpha_{ij}(\omega)). \tag{6}$$

Then, inversion of Eqs. (5) and (6) has been performed, writing frequency-dependent molecular polarizabilities as a function of the cross sections tensors. This method is much faster than the Sternheimer calculation mode [94], allowing also to use a PBE hybrid exchange–correlation functional in the TD-DFT calculations.

A thorough description of the OCTOPUS code and the different numerical implementations it uses can be found in original Refs. [91,92] (see also the dedicated web site, https://octopus-code.org/documentation/main).

3.2. Computational details

3.2.1. Ground state computation

The number of molecules constituting the database used to fit the frequency-dependent atomic polarizabilities with the reverse-DADI method should necessarily be limited because of the computation time which is required to calculate the frequency-dependent molecular polarizabilites with the TD-DFT calculations. Here, we will show that even a limited set of molecules may lead to accurate results, which thus represents one of the great advantage of our approach to calculate absorption cross sections.

Indeed, we have used the TD-DFT method to compute absorption cross sections between 1.5 and 20 eV for 12 molecules (7 PAHs and 5 alkanes), namely: anthanthrene ($C_{22}H_{12}$), benzo[a,e]pyrene ($C_{20}H_{12}$), benzoanthracene ($C_{18}H_{12}$), benzocoronene ($C_{28}H_{14}$), benzoperylene ($C_{22}H_{12}$), circumanthracene ($C_{40}H_{16}$), ethane (C_2H_6), propane (C_3H_8), butane (C_4H_{10}), pentane (C_5H_{12}), and hexane (C_6H_{14}).

These molecules have been chosen for their medium size and their atomic composition. Indeed, in this series of molecules, PAHs only contain 2 types of atoms, namely hydrogen atoms and carbon atoms with sp^2 hybridization (which will be called carbon C3 in the following, because these carbon atoms have 3 bonds with neighbors), whereas the alkanes are formed by a large number of hydrogen atoms and by carbon atoms with sp^3 hybridization (hereafter called carbons C4 because they have four neighbors). Note that the absorption cross sections for the selected PAHs have also been previously computed by Malloci et al. [95–97], so that the relevance of our results can be ensured by comparison.

For the TD-DFT calculations performed with Octopus, the cartesian coordinates of all the atoms forming the aromatic molecule have been directly taken from the PAH database made available by G. Malloci et al. [96,97], which contains optimized geometries obtained through the Gaussian-based DFT module of the NWChem code [98,99]. Note that, following the works of Langhoff [100], Bauschlicher & Langhoff [101], and Hudgins et al. [102], the hybrid exchange–correlation functional B3LYP [103,104] and the 6-31+G* [105] Gaussian basis sets have been used to expand the molecular orbitals in these calculations. For the alcanes, the initial geometries have been taken from the NIST CCCBDB [106], and optimized by DFT calculations performed with the B3LYP functional and the aug-cc-pVTZ basis set.

Unlike other common quantum chemistry softwares, Octopus uses an uniform grid in real space of a finite volume to solve the Kohn–Sham equations, that replaces the basis set in the calculation. That is, wavefunctions are represented by their value over a set of points in the real space. Two parameters are therefore needed to define the real-space discretization: the volume of the box and the spacing (which is the distance between two points of the mesh on which the functions will be evaluated). This spacing is a critical value. Indeed, as this parameter increases, the representation of functions degrades, and as it becomes smaller, the number of points increases, which in turn increases memory needs and computation time. Choosing an adequate box size is also crucial. In a too small box, the wavefunctions will be forced to go to zero unnaturally. By contrast, if the box is too large, a larger number of points is needed, increasing calculation time and memory requirements.

Here, because our own preliminary tests have shown that it is more economical in terms of computation time to use a cylindrical box rather than a spherical one, for the same radius (a saving of around 10% for the calculation of the Naphthalene and Anthracene spectra has been indeed obtained), all the subsequent calculations have been performed using also a cylindrical box, in which the molecule of interest stands. This has raised the question of choosing a radius and box height large enough for the simulation to provide accurate results. Octopus uses zero boundary conditions, i.e., wavefunctions and electron density are zero on the domain boundary. As the molecules are flat, we have considered it was sufficient to choose a height such that the molecule is placed at the center of the cylinder and the top and bottom edges are 4 Å apart above and below the molecule. On the other hand, the radius of the cylinder has been determined as a function of the radius of the molecule under consideration to obtain a converged spectrum within a reasonable calculation time. This has been done by selecting the minimum radius for which the total energy of the system converges. We have proceeded in the same way to determine the spacing. The results of this study show that it is sufficient to consider 6 Å between the lateral surface of the cylinder and the ends of the molecule. In other words, the convergence of the total energy is achieved for a cylinder with a radius equal to half the largest distance between two carbon atoms in the molecule under consideration, plus 6 Å. For the spacing, the same convergence study has been performed, showing a convergence of the spectra is reached for a value of 0.22 Å. For the two calculations steps, the Perdew, Burke & Ernzerhof (PBE0) exchange–correlation functional has been used [107].

3.2.2. Time dependent computation

In this step, the strength k of the delta (in time) perturbation applied to the molecule is defined. The electric field is modified, which causes the wavefunctions instantaneously to acquire a phase e^{ikx}. To keep the response linear and to avoid numerical problems, a value of $k = 0.01$ Å^{-1} has been chosen.

The problem to solve is therefore a set of Schrödinger-like equations for the electronic orbitals $\psi_j(t)$, written as

$$i\hbar \frac{\partial \psi_j(t)}{\partial t} = H(t)\psi_j(t), \tag{7}$$

and

$$\psi_j(t=0) = \psi_j^{(0)}. \tag{8}$$

Because Eq. (7) is linear (the time derivative and the Hamiltonian are both linear operators), one may formally define a linear "evolution" operator, $U(t)$, which transforms the initial vector into the solution at time t as

$$\psi_j(t) = U(t)\psi_j^{(0)}. \tag{9}$$

When the system is exposed to external time-dependent perturbations like electric and magnetic fields, the Hamiltonian does not commute with itself at different times anymore. To address this problem, Octopus discretizes the time-evolution operator and makes a discretized time-propagation of the orbital until self-consistency is reached. Here, the propagators defined as Approximated Enforced Time-Reversal Symmetry (AETRS) [108,109], that performs a second-order polynomial extrapolation of the discretized Hamiltonian, have been chosen to approximate the evolution operator.

A maximum propagation time of 10 $\hbar$/eV has been chosen and the time evolution has been performed using a time step of 0.0023 $\hbar$/eV, which ensured energy conservation with extremely good numerical accuracy. After repeating this calculation independently for the 3 Cartesian directions of the incident perturbation, the post-processing utility *oct-propagation_spectrum* has been used to compute the cross sections, using the variable *PropagationSpectrumTransform* = sine to produce spectrum of Eq. (5) and *PropagationSpectrumTransform* = cosine to produce spectrum of Eq. (6) which allow us to compute the imaginary and the real parts of the frequency-dependent molecular polarizabilities, respectively.

4. Results

4.1. Results of the reverse-DADI fitting procedure for carbon and hydrogen atoms

4.1.1. Fit on the PAH data

Considering first the 7 PAHs for which frequency-dependent molecular polarizabilities have been computed, the fitting procedure in the reverse-DADI method has been dedicated on getting values of hydrogen (isotropic) polarizability between 1.5 and 20 eV, i.e., a range of energy which corresponds to a range of wavelengths (going from 62 to 826 nm) of interest for atmospheric and interstellar sciences. To focus the fit on the hydrogen atoms only, atomic polarizability values coming from the set of parameters calculated from Draine's data [87–89] have been imposed for the carbon atoms. Thus, for each excitation energy, atomic polarizability values for hydrogens have been iteratively adjusted until the best match with the molecular polarizabilities previously calculated at the TD-DFT level has been obtained. The fitting procedure has been initialized using an isotropic polarizability value for hydrogen equal to $0.1 + i0.01$ Å^3. Then, for each given energy value, the starting point for the hydrogen polarizability has been chosen to be the value found for the previous energy.

Then, a second fitting procedure has been performed to get the frequency-dependent atomic polarizability values for carbon atoms in aromatic structures (C3), still between 1.5 and 20 eV, taking into account the presence of hydrogen bonds on the edges of the 7 PAH molecules considered in the TD-DFT calculations. In this procedure, the parameters for the hydrogen atoms have been imposed with values coming from the fit mentioned above. Focusing thus on the carbon atoms only, the fit has been initialized by using anisotropic carbon polarizabilities derived from Draine's graphite parametrization [87]. Then, the polarizability value obtained at a given energy has been chosen as a starting point for calculations at the next energy value.

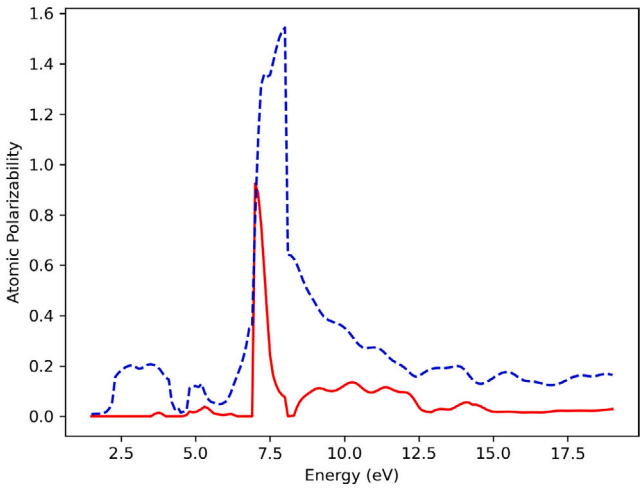

Fig. 1. Values (in Å^3) of the real (blue dashed curve) and imaginary (red curve) parts of the frequency-dependent atomic polarizability of H atoms in PAH molecules, calculated as a function of the energy, between 1.5 and 20 eV.

These successive fits have constituted one full step of our fitting procedure. Then, this step has been iteratively repeated (using the preceding values of the carbon polarizability rather than Draine's parameters) up to the convergence of the atomic polarizability values both for hydrogen and carbon atoms, which has been in fact quickly obtained, because only two full iterations have been necessary, as shown on Fig. S1 given in the Supplementary Information.

The results obtained for the frequency-dependent atomic polarizability (real and imaginary parts) of the H atoms are given in Fig. 1. Consistently with the physical intuition, these values are close to zero except around a resonance, observed between 7 and 8 eV.

The results of the reverse-DADI procedure for the C3 atoms are given on Fig. 2, where values of real and imaginary parts of the parallel and perpendicular components of the anisotropic frequency-dependent atomic polarizability tensor obtained here are also compared with those coming from Draine's parametrization of graphite [87].

This Figure clearly shows that, for the atomic polarizability tensor of C3 atoms, the values of the component parallel to the local carbon plane obtained with the reverse-DADI method are very similar to those calculated from Draine's data [87]. Much larger differences are evidenced when considering the component perpendicular to this local plane, a feature that could come from the fact that, in our calculations, the carbon atoms located at the edges of the PAH molecules are bound to hydrogen atoms, which is, of course, not the case in graphite. Moreover, this perpendicular component of the polarizability may be influenced by the stacking of the carbon sheets in graphite, a situation strongly different from that of isolated PAH, as in our work. In addition, as discussed by Draine and Lee [87], the experimental measurements of the dielectric function for the electric field perpendicular to the basal plane of graphite are not all mutually consistent and less reliable information is thus available regarding the perpendicular component of the polarizability tensor.

Finally, the atomic polarizabilities fitted for hydrogen and carbon (C3) atoms have been used to calculate, with the DADI model, the absorption cross sections of the 7 PAH molecules in the database, for

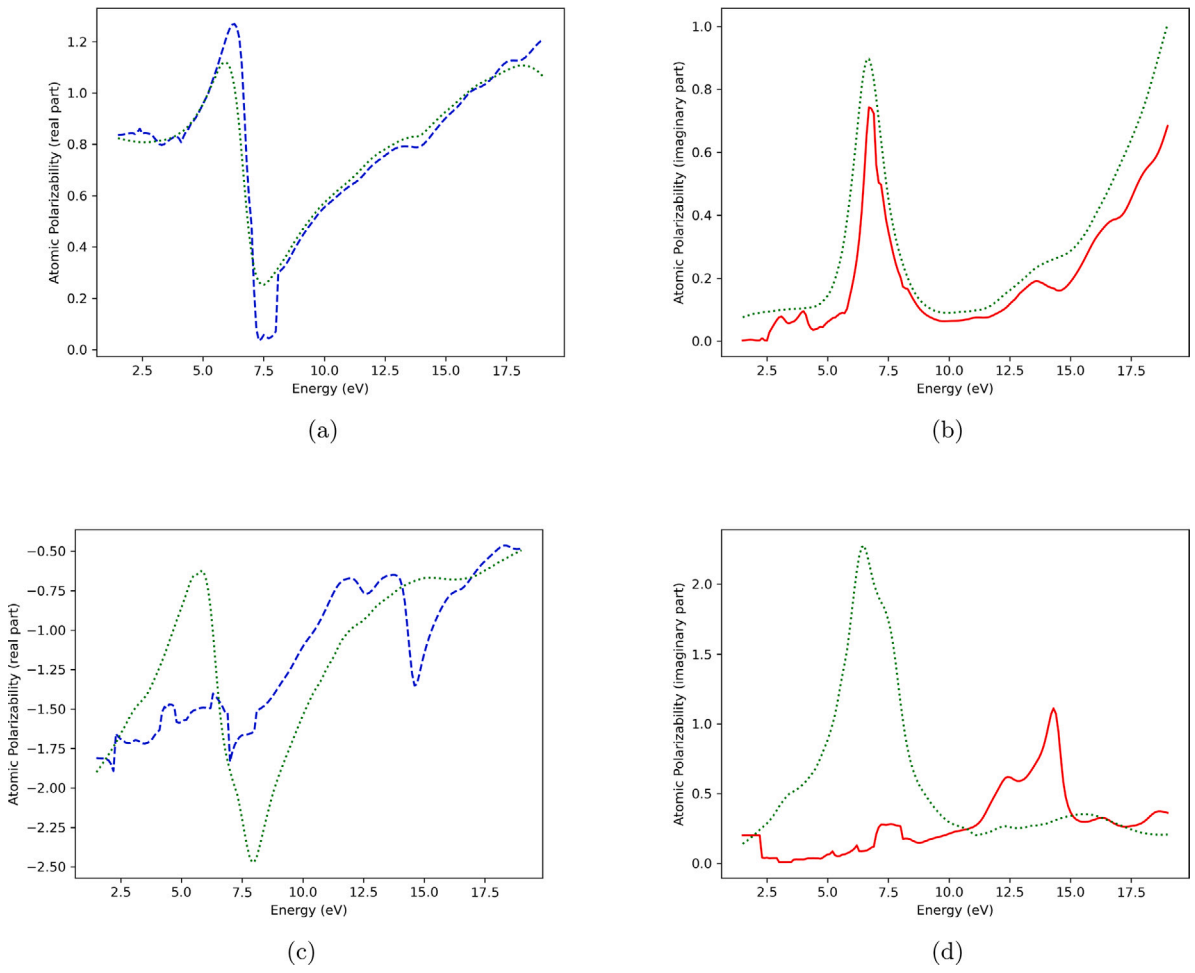

Fig. 2. Values (in Å^3) of the real (blue dashed curves in panels (a) and (c)) and imaginary (red curves in panels (b) and (d)) parts of the frequency-dependent atomic polarizability of carbon atoms (of C3 type) in PAH molecules, calculated as a function of the energy, between 1.5 and 20 eV. Parallel and perpendicular components of the polarizability tensor are given in the upper ((a) and (b)) and lower ((c) and (d)) panels, respectively. Note that on each graph, the data coming from the graphite parametrization [87] have also been given (green dotted curves), for comparison.

comparison with the TD-DFT reference data. The corresponding results are given in Fig. 3, which shows that the amplitude and position of the peaks computed with the DADI model (using the fitted atomic polarizability values as input) are very similar to the ones obtained by using the Octopus code (as evidenced by the correlation curve given on the vertical left panel). This is particularly true for the first peak of these curves, between 5 and 7 eV, for which the correspondence with the reference data is very good, a very important feature because this energy range corresponds to that of the $\pi - \pi^\star$ transitions due to sp^2 hybridization in carbonaceous structures [110] and to the prominent ultraviolet absorption feature (UV bump) observed in some galaxies [27,28,111].

To assess the convergence of our method, we have performed TD-DFT calculations for 5 more (larger) molecules, namely the dibenzocoronene ($C_{30}H_{14}$), the ovalene ($C_{32}H_{14}$), the circumpyrene ($C_{42}H_{16}$), the hexabenzocoronene ($C_{42}H_{18}$), and the dicoronylene ($C_{48}H_{20}$) molecules, which have thus been added to our initial set of 7 PAHs. Then, we have considered different numbers $N_0 = 5, 7, 12$ of PAH molecules in the database on which the atomic polarizabilities have been fitted, and we have evaluated the resulting mean deviation between the results of the absorption cross sections calculated with DADI and those obtained at the TD-DFT level with Octopus. This mean deviation δ has been defined as [61,70]:

$$\delta = \left[\frac{1}{n_{max}} \sum_{i=1}^{n_{max}} \frac{1}{N_0} \sum_{j=1}^{N_0} \left(\sigma_j^{DADI}(\omega_i) - \sigma_j^{TD-DFT}(\omega_i) \right)^2 \right]^{1/2} \quad (10)$$

where n_{max} is the maximum number of energy values considered in the calculations, within the range [1.5–20] eV.

The calculated values are $\delta = 0.93$ Å^2, $\delta = 0.43$ Å^2 and $\delta = 0.48$ Å^2, when considering 5, 7 and 12 HAPs in the database, respectively. This shows that increasing the database does not significantly improve the global results. For comparison, $\delta = 0.78$ Å^2 when using the Draine's parameters to calculate the absorption cross sections. More interestingly, we have obtained a value of $\delta = 0.45$ Å^2 between our own TD-DFT values and those calculated by Malloci et al. [97] with the B3LYP functional instead of the PBE0 one. We can thus conclude that using a relatively small database of 7 PAH molecules leads to differences in absorption cross sections between DADI and TD-DFT results that are, in average, no larger than the corresponding deviations obtained by using two different functionals in TD-DFT. Consequently, it may be reasonably thought that the 7 PAH molecules defining our initial database represent a sufficiently large set of molecules for relatively accurate fitting.

4.1.2. Fit on the alkane data

Another fitting procedure has been performed using the five alkane molecules in our database. These molecules contain carbon of type C4 (aliphatic carbons) and many hydrogen atoms. Using the same procedure as above, frequency-dependent atomic polarizabilities have been fitted for carbon (C4), imposing the above fitted values for the polarizability of the hydrogen atoms. An isotropic polarizability tensor

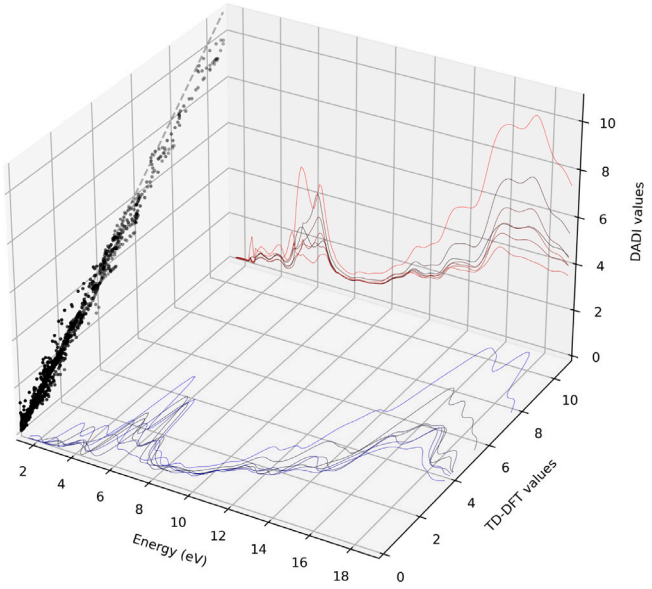

Fig. 3. Comparison between the absorption cross sections (in Å^2) of the initial set of 7 PAH molecules considered here (see text), as calculated with the DADI model using the atomic H and C polarizability values fitted in the present work as inputs (vertical panel, y_1) or with the TD-DFT method (horizontal panel, y_2), between 1.5 and 20 eV. The vertical left panel shows the correlation between DADI and TD-DFT results (where the straight line indicates the strict equality $y_1 = y_2$ between the DADI and TD-DFT values, at any given value of the energy).

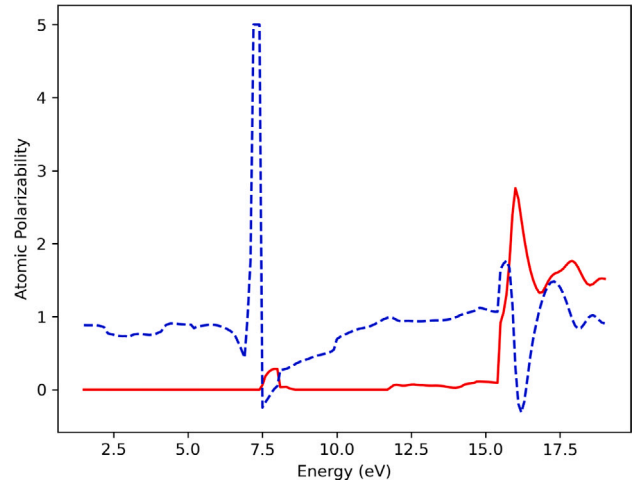

Fig. 4. Values (in Å^3) of the real (blue dashed curve) and imaginary (red curve) parts of the frequency-dependent atomic polarizability of aliphatic carbon (C4) atoms, calculated as a function of the energy, between 1.5 and 20 eV.

has thus been calculated for the C4 atoms, with an initialization of the values arbitrarily chosen to be $0.1 + i0.01$ Å^3. Again, at a given energy, the polarizability value obtained at the previous energy has been used as a starting point of the fitting procedure. The corresponding results for the isotropic polarizability of C4 atoms are shown Fig. 4.

As can be seen in this Figure, the imaginary part of the polarizability, which is mainly responsible for the absorption features, remains always close to zero, except around 8 eV where a small peak is evidenced, and above 15.5 eV, a region which thus could correspond to stronger absorption.

Unfortunately, as for the hydrogen atoms, we are not aware of any experimental data for the frequency-dependent atomic polarizability of aliphatic carbons that can be used as reference for comparison.

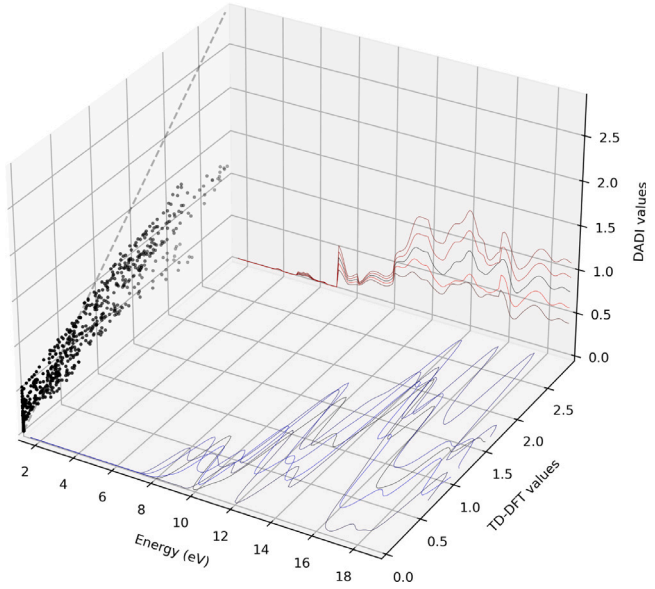

Fig. 5. Comparison between the absorption cross sections (in Å^2) of a set of 5 alkane molecules (see text) as calculated with the DADI model using the atomic H (aromatic) and C (C4) polarizability values fitted in the present work as inputs (vertical panel, y_1) or with the TD-DFT method (horizontal panel, y_2), between 1.5 and 20 eV. The vertical left panel shows the correlation between DADI and TD-DFT results (the straight line indicates the strict equality $y_1 = y_2$ between the two sets of values).

In a second step, the atomic polarizabilities given in Fig. 4 have been used together with those previously obtained for the hydrogen atoms (see Fig. 1) in the DADI model to compute the absorption cross sections of the five alkane molecules of our database and to compare the corresponding results with those coming from the TD-DFT calculations (see Fig. 5).

As it can be seen on the left vertical panel of Fig. 5, the correlation between the results obtained with the DADI model and with the TD-DFT is not very satisfactory (at least, it is less good than the correlation exhibited on Fig. 3 for the PAH molecules). However, it should be recalled that, at this stage of our calculations, the atomic polarizability values for hydrogen have been taken from the results of the fit based on the PAH molecules. Thus, the present results indicate that the atomic polarizability of the hydrogens actually depends on the electron reservoir of their environment, which is clearly different between an aromatic cycle and an aliphatic chain. Then, it appeared more relevant to fit another isotropic atomic polarizability for hydrogen atoms, specifically suitable for aliphatic chains. Thus, a new fitting procedure has been performed, based on the alkane molecules, in which the atomic polarizability values of the carbons have been chosen as being those calculated for the C4 atoms, the only fitted parameters being those of the aliphatic hydrogens. The corresponding results are given in Fig. 6.

A quick comparison of these results with those given in Fig. 1 immediately shows that, indeed, the atomic polarizability values of aliphatic hydrogens are very different from those of aromatic hydrogens.

Considering these new parameters, the absorption cross sections for alkane molecules have been recalculated, and the results obtained with the DADI method and with the TD-DFT approach are compared in Fig. 7.

As it can be seen, the results are now clearly closer than before (see Fig. 5), as shown by the much better correlation, especially for energy values below 10 eV. This is also evidenced by the calculated values of the mean deviation with respect to TD-DFT absorption cross sections for this set of 5 alkane molecules, which are $\delta = 0.51$ Å^2 and $\delta = 0.28$ Å^2, when considering the atomic polarizability values of C4 atoms combined with those of either aromatic or aliphatic hydrogen atoms,

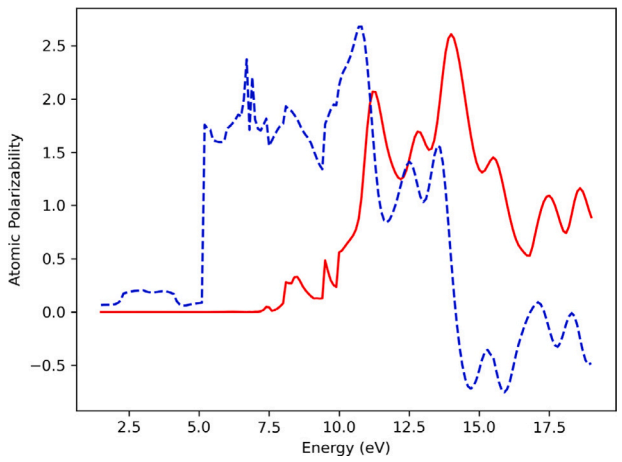

Fig. 6. Values (in Å^3) of the real (blue dashed curve) and imaginary (red curve) parts of the frequency-dependent atomic polarizability of H atoms in alkane molecules, calculated as a function of the energy, between 1.5 and 20 eV.

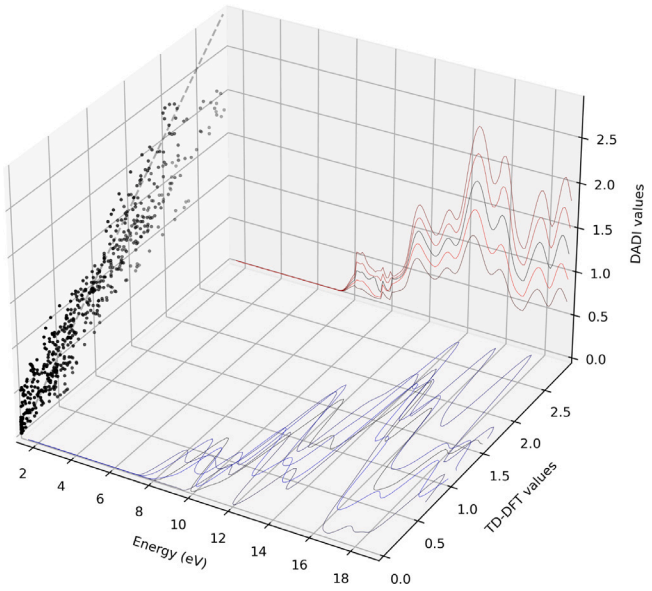

Fig. 7. Comparison between the absorption cross sections (in Å^2) of a set of 5 alkane molecules as calculated with the DADI model using the atomic H (aliphatic) and C (C4) polarizability values fitted in the present work as inputs (vertical panel, y_1) or with the TD-DFT method (horizontal panel, y_2), between 1.5 and 20 eV. The vertical left panel shows the correlation between DADI and TD-DFT results (the straight line indicates the strict equality $y_1 = y_2$ between the two sets of values).

respectively. This led us to consider that the frequency-dependent atomic polarizabilities obtained for aliphatic hydrogens and aliphatic carbons (C4) are accurate enough for not going further in improving their fitted values.

At this stage of our study, thanks to the reverse-DADI method, we now have at our disposal frequency-dependent atomic polarizability values, in the energy range between 1.5 and 20 eV, for four types of atoms that are usually involved in carbonaceous nanostructures of atmospheric or instellar environments, namely aromatic-like and aliphatic carbon (i.e., C3 and C4) and hydrogen (bound to C3 and C4) atoms.

4.2. Transferability of the fitted parameters

To test the transferability of the frequency-dependent atomic polarizabilities calculated above, the DADI method has been applied to compute the absorption cross sections of two large PAH molecules (ovalene ($C_{32}H_{14}$) and circumcoronene ($C_{54}H_{18}$)) that were not included in the fitting procedure performed in the reverse-DADI method with the initial database containing 7 PAHs. The corresponding results are given on Fig. 8, together with the absorption cross sections computed with the TD-DFT method, for comparison.

As it can be seen, results from DADI are in fair agreement with the TD-DFT ones on the whole range of energy considered here (that is between 1.5 and 20 eV), thus validating our fitted frequency-dependent atomic polarizabilities for aromatic molecules.

Moreover, we have also compared DADI calculations of the absorption cross sections performed with the frequency-dependent atomic polarizability values fitted on a database containing either 5, or 7, or 12 PAH molecules, as already explained above. The corresponding results are given in the Supplementary Information for the coronene molecule, which has been chosen as an illustration because it has not been included in any of the initial databases (see Fig. S2). In each case, the DADI results fairly agree with the absorption cross section calculated at the TD-DFT level, illustrating that all the 3 sets of PAH molecules may lead to acceptable results, although the calculations of the mean deviation δ appear to show that the initial database including 7 PAH molecules gives the best results, as indicated above. In addition, by considering the position of the first absorption peak calculated around 6 eV, a shift no larger than 0.5 eV is obtained between the three sets of calculations. This could be seen as rough estimate of the uncertainties inherent in the size of the initial base of PAH molecules on the DADI calculations.

In a similar way, the DADI model has also been used to compute the absorption cross sections of octane (C_8H_{18}), a molecule that was not involved in the fit of the atomic polarizability of aliphatic carbon (C4) and hydrogen atoms. Calculations have been performed by considering the atomic polarizability fitted for aromatic (see Fig. 1) and for aliphatic (see Fig. 6) hydrogens, for comparison, and the corresponding results are shown on Fig. 9, together with the results obtained by using the TD-DFT method.

As exhibited on Fig. 9, differences between the two DADI computations (i.e., by considering the atomic polarizability of either aromatic or aliphatic hydrogen) are observed over all spectral range. In addition, it should be noted that when using the atomic polarizability of the aromatic hydrogen, a peak at 7 eV appears in the spectrum, which is not at all evidenced when considering the polarizability of aliphatic hydrogens nor with the TD-DFT computations. By contrast, the atomic polarizability values obtained in our fitting procedure when considering hydrogen atoms involved in aliphatic chains give much more consistent results, especially below 12.5 eV. At higher energy, the global behavior of the calculations performed with the DADI model are also in a better agreement with the one of the TD-DFT results when using the atomic polarizabilities of aliphatic rather than those of aromatic hydrogen atoms, although the results obtained with the DADI model appear blue-shifted with respect to those obtained with the TD-DFT method.

Of course, this nice agreement between the absorption cross sections calculated with the DADI model and those coming from TD-DFT calculations for the circumcoronene, ovalene and octane molecules, allows to especially assess the accuracy of the imaginary part of the frequency-dependent polarizability. However, it is worth mentioning that similar fair agreement is also observed when considering the real parts of the molecular polarizability tensors, as shown in Fig. S3 given as Supplementary Information.

Finally, to complete our study, we have also applied our model to the computation of the absorption cross-sections of the 1-methylpyrene ($C_{17}H_{12}$) molecule, which contains both aromatic and aliphatic atoms. Calculations with the DADI model have thus been performed by using the frequency-dependent polarizabilities fitted for aliphatic and for aromatic atoms (and assigned to each of them depending on its neighborhood in the molecule). The results of these calculations are given in Fig. 10 together with those obtained by TD-DFT, for comparison.

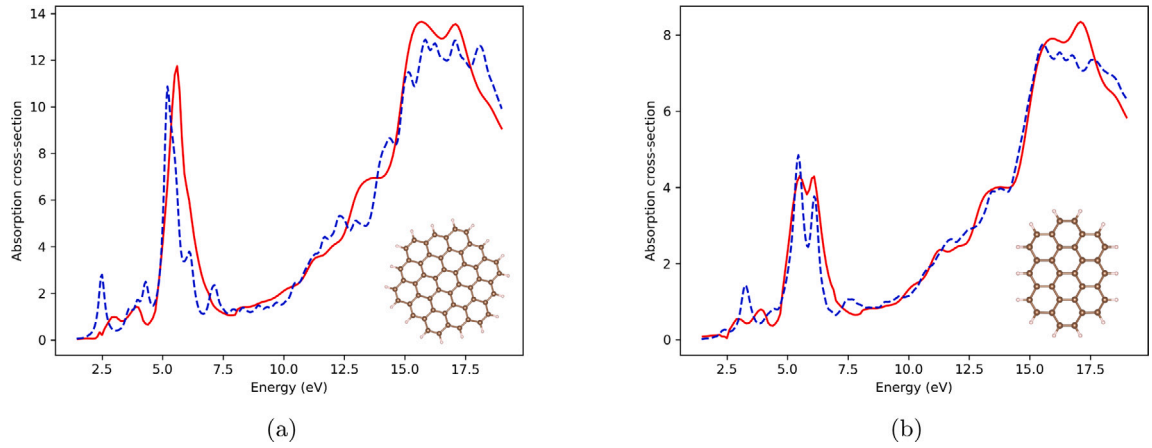

Fig. 8. Values of the absorption cross sections (in Å^2) of circumcoronene (left panel) and ovalene (right panel), calculated as a function of the energy, between 1.5 and 20 eV, with the DADI model (red curves) or with the TD-DFT method (blue dashed curves). A representation of the molecule (circumcoronene and ovalene) is also shown in the corresponding panel, for information.

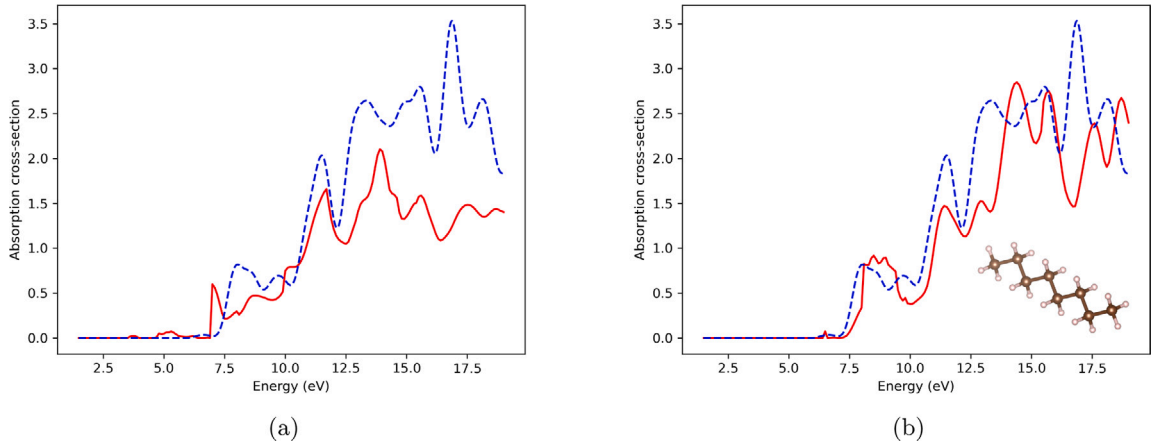

Fig. 9. Values of the absorption cross sections (in Å^2) of octane, calculated as a function of the energy, between 1.5 and 20 eV, with the DADI model (red curve) or with the TD-DFT method (blue dashed curve). Notice that, in the DADI calculations, the atomic polarizability of either (a) aromatic (left hand side of the Figure) or (b) aliphatic (right hand side) hydrogen atoms have been considered, for comparison. A representation of the octane molecule is also shown in panel (b), for information.

As it can be seen, a nice proper match is found between the TD-DFT cross-section and the one computed with our DADI model, over the whole spectral range with, however, an apparent global shift of about 0.4 eV between the two curves. This fair agreement, obtained for a large molecule which contains 4 different types of atoms (C3 and C4 carbon atoms, and aromatic and aliphatic hydrogen atoms), combined to the previous conclusions based on the results presented above for ovalene, circumcoronene and octane, emphasizes the robustness and transferability of the fitted frequency-dependent atomic polarizabilities resulting from the reverse-DADI method. Of course, these values of the polarizabilities are certainly not rigorously exact because the fitting method, the size of the learning set, and even the intrinsic (not known!) uncertainties of the TD-DFT results on which the parameters of the fits have been tuned may lead to uncertainties on the fitted parameters. However, as shown by the calculations of the mean deviations, differences between the absorption cross sections obtained within the DADI scheme and those coming from TD-DFT calculations are of the same order of magnitude as the deviations between TD-DFT calculations performed with different functionals and basis sets. Moreover, increasing the number of molecules that are included in the database on which the reverse-DADI calculations is based does not significantly change this conclusion, giving us confidence on the results given here.

It is worth noting, however, that the above results are all the more interesting as the total computation time for getting the polarizabilities and the absorption cross sections with reverse-DADI and DADI is very much shorter than with any quantum chemistry computation. Typically, with Octopus, the order of magnitude for TD-DFT computations of the absorption cross section for such large molecules is the day, whereas it is about one minute with the DADI method ! As a consequence, considering the consistency of our results, one can see the benefit of using the present fitted parameters to calculate, with the DADI method, the absorption spectrum of large molecules whose size prevents using any quantum-based method such as TD-DFT. This opens the perspective of creating a database of absorption spectra for carbonaceous species containing thousands of atoms of different types, which could be useful for identification of, e.g., relevant molecules in astrophysical environments.

5. Conclusion

Here, thanks to the reverse-DADI method, the frequency-dependent atomic polarizabilities of carbon and hydrogen atoms involved in aromatic cycles or in aliphatic chains, have been calculated for the first time. Using this fitted polarizabilities and the DADI model, absorption cross-sections have then been computed for PAHs and alkanes that were involved in the fitting procedure, in order to check self-consistency by comparing these results with those obtained by TD-DFT approach (using Octopus). In addition, to confirm the transferability of our approach, such a comparison has also been done for PAH

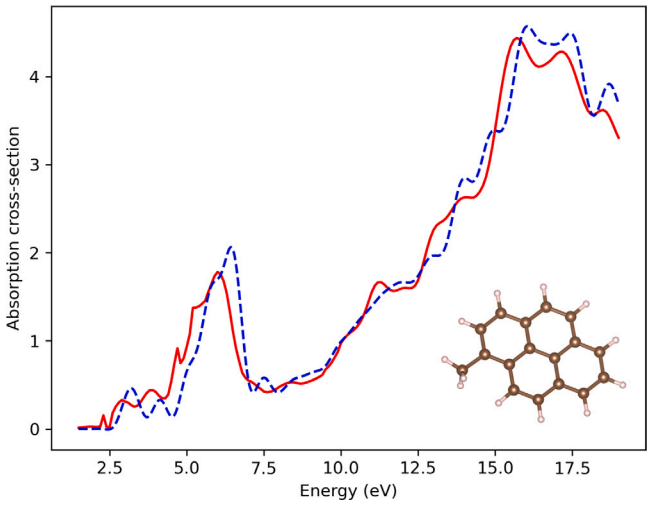

Fig. 10. Values of the absorption cross sections (in Å^2) of 1-methylpyrene, calculated as a function of the energy, between 1.5 and 20 eV, either with the DADI model (red curve) or with the TD-DFT method (blue dashed curve) for comparison. A representation of the 1-methylpyrene molecule is also shown in the figure, for information.

and alkane molecules that were not included in the fit, and by considering a molecule which contains all the types of atoms involved here (i.e., aliphatic and aromatic C and H). In each situation, a nice agreement has been evidenced between absorption cross-sections coming from the DADI model and from the TD-DFT computations. This agreement is all the more emphasizable as it has been obtained even starting from a very limited number of molecules in the initial database coming from the quantum calculations, thus needing a very limited computational cost.

We can therefore reasonably conclude that the values of the frequency-dependent atomic polarizabilities determined here, for the different atom types, may actually be used to compute optical properties of larger carbonaceous compounds of atmospheric and interstellar interests such as large PAHs, on the basis of their atomistic details, through the DADI model. Although results obtained with this approach are certainly not rigorously exact, we have shown that the differences between results obtained with the DADI approach and those coming from TD-DFT calculations are no larger than those obtained with TD-DFT performed with different functionals and basis sets, but with the great advantage of a much smaller computer cost. At this stage, the results presented here can thus be viewed as a nice first approach which, however, will require further calculations to include other molecules in the initial database that contain, for instance, other carbon hybridization or environments. Also, it is worth mentioning that the frequency-dependent atomic polarizability values fitted here for aromatic carbon atoms have been calculated for flat structures (PAHs), only. Thus, curvature effects may prevent using the present values to compute the optical properties of fullerene-like species. More specifically, it is known that resonances are visible before the first absorption peak for fullerene, that do not exist for planar structures.

CRediT authorship contribution statement

N. Brosseau-Habert: Writing – original draft, Investigation, Formal analysis, Data curation. **F. Miradji:** Software, Methodology. **S. Picaud:** Writing – original draft, Validation, Supervision, Project administration, Funding acquisition, Formal analysis. **M. Devel:** Supervision, Software, Project administration, Methodology, Funding acquisition, Conceptualization.

Declaration of competing interest

The authors declare that they have no known competing financial interests or personal relationships that could have appeared to influence the work reported in this paper.

Data availability

Data will be made available on request.

Acknowledgments

This work has been supported by the EIPHI Graduate School (contract ANR-17-EURE-0002) and the Région Bourgogne-Franche-Comté. Computations have been performed on local facilities of Institut FEMTO-ST and on the regional supercomputer facilities of the Mésocentre de calcul de Franche-Comté. We thank Prof. Clément Dombry (Laboratoire de Mathematiques - Besançon) for fruitful discussions on the accuracy of the fitting methods tested in the present work.

Appendix A. Supplementary data

Supplementary material related to this article can be found online at https://doi.org/10.1016/j.jqsrt.2024.109194.

References

[1] Jaramillo P, Kahn Ribeiro S, Newman P, Dhar S, Diemuodeke O, Kajino T, Lee D, Nugroho S, Ou X, Hammer Strømman A, Whitehead J. Transport. In: Shukla P, Skea J, Slade R, Khourdajie AA, van Diemen R, McCollum D, Pathak M, Some S, Vyas P, Fradera R, Belkacemi M, Hasija A, Lisboa G, Luz S, Malley J, editors. Climate change 2022: mitigation of climate change. Contribution of working group III to the sixth assessment report of the intergovernmental panel on climate change. Cambridge, UK and New York, NY, USA: Cambridge University Press; 2022, p. 1049–160. http://dx.doi.org/10.1017/9781009157926.012.

[2] Zhang H, Wang Z. Advances in the study of black carbon effects on climate. Adv Clim Change Res 2011;2(1):23–30. http://dx.doi.org/10.3724/SP.J.1248.2011.00023.

[3] Bond TC, Doherty SJ, Fahey DW, Forster PM, Berntsen T, DeAngelo BJ, Flanner MG, Ghan S, Kärcher B, Koch D, et al. Bounding the role of black carbon in the climate system: A scientific assessment. J Geophys Res: Atmos 2013;118(11):5380–552. http://dx.doi.org/10.1002/jgrd.50171.

[4] Lohmann U, Friebel F, Kanji ZA, Mahrt F, Mensah AA, Neubauer D. Future warming exacerbated by aged-soot effect on cloud formation. Nat Geosci 2020;13(10):674–80. http://dx.doi.org/10.1038/s41561-020-0631-0.

[5] Lu Q, Liu C, Zhao D, Zeng C, Li J, Lu C, Wang J, Zhu B. Atmospheric heating rate due to black carbon aerosols: Uncertainties and impact factors. Atmos Res 2020;240:104891. http://dx.doi.org/10.1016/j.atmosres.2020.104891.

[6] Bessagnet B, Allemand N, Putaud J-P, Couvidat F, André J-M, Simpson D, Pisoni E, Murphy BN, Thunis P. Emissions of carbonaceous particulate matter and ultrafine particles from vehicles—a scientific review in a cross-cutting context of air pollution and climate change. Appl Sci 2022;12(7):3623. http://dx.doi.org/10.3390/app12073623.

[7] Janssen NA, Gerlofs-Nijland ME, Lanki T, Salonen RO, Cassee F, Hoek G, Fischer P, Brunekreef B, Krzyzanowski M. Health effects of black carbon. World Health Organization. Regional Office for Europe; 2012.

[8] Ali MU, Siyi L, Yousaf B, Abbas Q, Hameed R, Zheng C, Kuang X, Wong MH. Emission sources and full spectrum of health impacts of black carbon associated polycyclic aromatic hydrocarbons (PAHs) in urban environment: A review. Crit Rev Environ Sci Technol 2021;51(9):857–96. http://dx.doi.org/10.1080/10643389.2020.1738854.

[9] Wang R, Balkanski Y, Boucher O, Ciais P, Schuster GL, Chevallier F, Samset BH, Liu J, Piao S, Valari M, et al. Estimation of global black carbon direct radiative forcing and its uncertainty constrained by observations. J Geophys Res: Atmos 2016;121(10):5948–71. http://dx.doi.org/10.1002/2015JD024326.

[10] Koch D, Del Genio A. Black carbon semi-direct effects on cloud cover: Review and synthesis. Atmos Chem Phys 2010;10(16):7685–96. http://dx.doi.org/10.5194/acp-10-7685-2010.

[11] Ohlwein S, Kappeler R, Kutlar Joss M, Künzli N, Hoffmann B. Health effects of ultrafine particles: A systematic literature review update of epidemiological evidence. Int J Public Health 2019;64:547–59. http://dx.doi.org/10.1007/s00038-019-01202-7.

[12] Schraufnagel DE. The health effects of ultrafine particles. Exp Mol Med 2020;52(3):311–7. http://dx.doi.org/10.1038/s12276-020-0403-3.

[13] Lahaye J, Prado G. Morphology and internal structure of soot and carbon blacks. In: Siegla DC, Smith GW, editors. Particulate carbon: formation during combustion. Boston, MA: Springer US; 1981, p. 33–55. http://dx.doi.org/10.1007/978-1-4757-6137-5-2.
[14] Kahnert M, Devasthale A. Black carbon fractal morphology and short-wave radiative impact: A modelling study. Atmos Chem Phys 2011;11(22):11745–59. http://dx.doi.org/10.5194/acp-11-11745-2011.
[15] Donnet J-B. Carbon black: Science and technology. Routledge; 2018.
[16] Cataldo F, Pontier-Johnson MA. Recent discoveries in carbon black formation and morphology and their implications on the structure of interstellar carbon dust. Fuller Nanotubes Carbon Nanostruct 2002;10(1):1–14. http://dx.doi.org/10.1081/FST-120002925.
[17] Wang S, Li A, Jiang B. Modeling the infrared interstellar extinction. Planet Space Sci 2014;100:32–9. http://dx.doi.org/10.1016/j.pss.2014.03.018.
[18] Mousis O, Lunine J, Petit J-M, Zahnle K, Biennier L, Picaud S, Johnson T, Mitchell JBA, Boudon V, Cordier D, et al. On the volatile enrichments and heavy element content in HD189733b. Astrophys J 2011;727(2):77. http://dx.doi.org/10.1088/0004-637X/727/2/77.
[19] Venot O, Hébrard E, Agúndez M, Decin L, Bounaceur R. New chemical scheme for studying carbon-rich exoplanet atmospheres. Astron Astrophys 2015;577:A33. http://dx.doi.org/10.1051/0004-6361/201425311.
[20] Lavvas P, Koskinen T. Aerosol properties of the atmospheres of extrasolar giant planets. Astrophys J 2017;847(1):32. http://dx.doi.org/10.3847/1538-4357/aa88ce.
[21] Gao P, Wakeford HR, Moran SE, Parmentier V. Aerosols in exoplanet atmospheres. J Geophys Res: Planets 2021;126(4):e2020JE006655. http://dx.doi.org/10.1029/2020JE006655.
[22] Verstraete L, Pech C, Moutou C, Wright C, Drapatz S, Léger A, Sellgren K. The aromatic infrared bands as seen by ISO: probing the PAH model. In: ISO beyond the peaks: the 2nd ISO workshop on analytical spectroscopy. Vol. 456, 2000, p. 319.
[23] Tielens A. Interstellar polycyclic aromatic hydrocarbon molecules. Annu Rev Astron Astrophys 2008;46(1):289–337. http://dx.doi.org/10.1146/annurev.astro.46.060407.145211.
[24] Chen T, Luo Y, Li A. The infrared bands of polycyclic aromatic hydrocarbons in the 1.6–1.7 μm wavelength region. Astron Astrophys 2019;632:A71. http://dx.doi.org/10.1051/0004-6361/201936310.
[25] Herbig GH. The diffuse interstellar bands. Annu Rev Astron Astrophys 1995;33(1):19–73. http://dx.doi.org/10.1146/annurev.aa.33.090195.000315.
[26] Ehrenfreund P. The diffuse interstellar bands as evidence for polyatomic molecules in the diffuse interstellar medium. In: American astronomical society meeting abstracts# 194. Vol. 194, 1999, p. 41–01.
[27] Stecher TP. Interstellar extinction in the ultraviolet. Astrophys J 1965;142:1683, vol. 142, p. 1683.
[28] Fitzpatrick E, Massa D. An analysis of the shapes of interstellar extinction curves. V. The IR-through-UV curve morphology. Astrophys J 2007;663(1):320. http://dx.doi.org/10.1086/518158.
[29] Zafar T, Heintz K, Fynbo J, Malesani D, Bolmer J, Ledoux C, Arabsalmani M, Kaper L, Campana S, Starling R, et al. The 2175Å extinction feature in the optical afterglow spectrum of GRB 180325A at $z = 2.25$. Astrophys J Lett 2018;860(2):L21. http://dx.doi.org/10.3847/2041-8213/aaca3f.
[30] Jones A, Fanciullo L, Köhler M, Verstraete L, Guillet V, Bocchio M, Ysard N. The evolution of amorphous hydrocarbons in the ISM: Dust modelling from a new vantage point. Astron Astrophys 2013;558:A62. http://dx.doi.org/10.1051/0004-6361/201321686.
[31] Micelotta ER, Jones AP, Cami J, Peeters E, Bernard-Salas J, Fanchini G. The formation of cosmic fullerenes from arophatic clusters. Astrophys J 2012;761(1):35. http://dx.doi.org/10.1088/0004-637X/761/1/35.
[32] Zhen J, Castellanos P, Paardekooper DM, Linnartz H, Tielens AG. Laboratory formation of fullerenes from PAHs: top-down interstellar chemistry. Astrophys J Lett 2014;797(2):L30. http://dx.doi.org/10.1088/2041-8205/797/2/L30.
[33] Berné O, Montillaud J, Joblin C. Top-down formation of fullerenes in the interstellar medium. Astron Astrophys 2015;577:A133. http://dx.doi.org/10.1051/0004-6361/201425338.
[34] Roy A, Surendra V, Ramachandran R, Meka J, Gupta S, Janardhan P, Rajasekhar B, Hill H, Bhardwaj A, Mason N, et al. Interstellar carbonaceous dust and its formation pathways: From an experimental astrochemistry perspective. J Indian Inst Sci 2023;103(3):919–38. http://dx.doi.org/10.1007/s41745-023-00393-6.
[35] Kahnert M, Kanngießer F. Modelling optical properties of atmospheric black carbon aerosols. J Quant Spectrosc Radiat Transfer 2020;244:106849. http://dx.doi.org/10.1016/j.jqsrt.2020.106849.
[36] Moosmüller H. Optical properties of nonspherical, light-absorbing particles: Black carbon and mineral dust aerosols. In: Light, plasmonics and particles. Elsevier; 2023, p. 349–69.
[37] Bond TC, Bergstrom RW. Light absorption by carbonaceous particles: An investigative review. Aerosol Sci Technol 2006;40(1):27–67. http://dx.doi.org/10.1080/02786820500421521.
[38] Sorensen C. Light scattering by fractal aggregates: A review. Aerosol Sci Technol 2001;35(2):648–87. http://dx.doi.org/10.1080/02786820117868.
[39] Yon J, Rozé C, Girasole T, Coppalle A, Méès L. Extension of RDG-FA for scattering prediction of aggregates of soot taking into account interactions of large monomers. Part Part Syst Charact 2008;25(1):54–67. http://dx.doi.org/10.1002/ppsc.200700011.
[40] Yon J, Liu F, Bescond A, Caumont-Prim C, Rozé C, Ouf F-X, Coppalle A. Effects of multiple scattering on radiative properties of soot fractal aggregates. J Quant Spectrosc Radiat Transfer 2014;133:374–81. http://dx.doi.org/10.1016/j.jqsrt.2013.08.022.
[41] Mishchenko MI, Travis LD, Mackowski DW. T-matrix computations of light scattering by nonspherical particles: A review. J Quant Spectrosc Radiat Transfer 1996;55(5):535–75. http://dx.doi.org/10.1016/0022-4073(96)00002-7.
[42] Bi L, Yang P. Accurate simulation of the optical properties of atmospheric ice crystals with the invariant imbedding T-matrix method. J Quant Spectrosc Radiat Transfer 2014;138:17–35. http://dx.doi.org/10.1016/j.jqsrt.2014.01.013.
[43] Mishchenko MI. Comprehensive thematic T-matrix reference database: A 2017–2019 update. J Quant Spectrosc Radiat Transfer 2020;242:106692. http://dx.doi.org/10.1016/j.jqsrt.2019.106692.
[44] Draine BT. The discrete-dipole approximation and its application to interstellar graphite grains. Astrophys J 1 1988;333:848–72. http://dx.doi.org/10.1086/166795.
[45] Draine BT, Flatau PJ. Discrete-dipole approximation for scattering calculations. J Opt Soc Amer A 1994;11(4):1491–9. http://dx.doi.org/10.1364/JOSAA.11.001491.
[46] Yurkin MA, Hoekstra AG. The discrete dipole approximation: an overview and recent developments. J Quant Spectrosc Radiat Transfer 2007;106(1–3):558–89. http://dx.doi.org/10.1016/j.jqsrt.2007.01.034.
[47] Chaumet PC. The discrete dipole approximation: A review. Mathematics 2022;10(17):3049. http://dx.doi.org/10.3390/math10173049.
[48] Yurkin MA. Discrete dipole approximation. In: Light, plasmonics and particles. Elsevier; 2023, p. 167–98.
[49] Parent P, Laffon C, Marhaba I, Ferry D, Regier T, Ortega I, Chazallon B, Carpentier Y, Focsa C. Nanoscale characterization of aircraft soot: A high-resolution transmission electron microscopy, Raman spectroscopy, X-ray photoelectron and near-edge X-ray absorption spectroscopy study. Carbon 2016;101:86–100. http://dx.doi.org/10.1016/j.carbon.2016.01.040.
[50] Adachi K, Chung SH, Buseck PR. Shapes of soot aerosol particles and implications for their effects on climate. J Geophys Res: Atmos 2010;115(D15). http://dx.doi.org/10.1029/2009JD012868.
[51] Eggersdorfer ML, Kadau D, Herrmann HJ, Pratsinis SE. Aggregate morphology evolution by sintering: Number and diameter of primary particles. J Aerosol Sci 2012;46:7–19. http://dx.doi.org/10.1016/j.jaerosci.2011.11.005.
[52] Bescond A, Yon J, Girasole T, Jouen C, Rozé C, Coppalle A. Numerical investigation of the possibility to determine the primary particle size of fractal aggregates by measuring light depolarization. J Quant Spectrosc Radiat Transfer 2013;126:130–9. http://dx.doi.org/10.1016/j.jqsrt.2012.10.011.
[53] Yon J, Bescond A, Liu F. On the radiative properties of soot aggregates part 1: Necking and overlapping. J Quant Spectrosc Radiat Transfer 2015;162:197–206. http://dx.doi.org/10.1016/j.jqsrt.2015.03.027.
[54] Bescond A, Yon J, Ouf F-X, Rozé C, Coppalle A, Parent P, Ferry D, Laffon C. Soot optical properties determined by analyzing extinction spectra in the visible near-UV: Toward an optical speciation according to constituents and structure. J Aerosol Sci 2016;101:118–32. http://dx.doi.org/10.1016/j.jaerosci.2016.08.001.
[55] Doner N, Liu F, Yon J. Impact of necking and overlapping on radiative properties of coated soot aggregates. Aerosol Sci Technol 2017;51(4):532–42. http://dx.doi.org/10.1080/02786826.2016.1275513.
[56] Liu F, Yon J, Bescond A. On the radiative properties of soot aggregates–part 2: Effects of coating. J Quant Spectrosc Radiat Transfer 2016;172:134–45. http://dx.doi.org/10.1016/j.jqsrt.2015.08.005.
[57] Qi H, Picaud S, Devel M, Liang E, Wang Z. Adsorption of organic molecules on onion-like carbons: insights on the formation of interstellar hydrocarbons. Astrophys J 2018;867(2):133. http://dx.doi.org/10.3847/1538-4357/aae4e4.
[58] Hanine M, Meng Z, Lu S, Xie P, Picaud S, Devel M, Wang Z. Formation of interstellar complex polycyclic aromatic hydrocarbons: Insights from molecular dynamics simulations of dehydrogenated benzene. Astrophys J 2020;900(2):188. http://dx.doi.org/10.3847/1538-4357/abab06.
[59] Applequist J, Carl JR, Fung K-K. Atom dipole interaction model for molecular polarizability. Application to polyatomic molecules and determination of atom polarizabilities. J Am Chem Soc 1972;94(9):2952–60.
[60] Applequist J. An atom dipole interaction model for molecular optical properties. Acc Chem Res 1977;10(3):79–85.
[61] Applequist J. Atom charge transfer in molecular polarizabilities: application of the olson-sundberg model to aliphatic and aromatic hydrocarbons. J Phys Chem 1993;97(22):6016–23. http://dx.doi.org/10.1021/j100124a039.
[62] Jensen L, Åstrand P-O, Sylvester-Hvid KO, Mikkelsen KV. Frequency-dependent molecular polarizability calculated within an interaction model. J Phys Chem A 2000;104(7):1563–9.

[63] Mayer A, Lambin P, Åstrand P. An electrostatic interaction model for frequency-dependent polarizability: Methodology and applications to hydrocarbons and fullerenes. Nanotechnology 2008;19(2):025203.

[64] Shanker B, Applequist J. Polarizabilities of fullerenes C_{20} through C_{240} from atom monopole-dipole interaction theory. J Phys Chem 1994;98(26):6486–9.

[65] Mayer A, Lambin P, Langlet R. Charge-dipole model to compute the polarization of fullerenes. Appl Phys Lett 2006;89(6):063117.

[66] Mayer A. Formulation in terms of normalized propagators of a charge-dipole model enabling the calculation of the polarization properties of fullerenes and carbon nanotubes. Phys Rev B 2007;75(4):045407.

[67] Jensen L, Schmidt OH, Mikkelsen KV, Åstrand P-O. Static and frequency-dependent polarizability tensors for carbon nanotubes. J Phys Chem B 2000;104(45):10462–6. http://dx.doi.org/10.1021/jp994073k.

[68] Mayer A. A monopole-dipole model to compute the polarization of metallic carbon nanotubes. Appl Phys Lett 2005;86(15):153110.

[69] Mayer A, Åstrand P-O. A charge-dipole model for the static polarizability of nanostructures including aliphatic, olephinic, and aromatic systems. J Phys Chem A 2008;112(6):1277–85.

[70] Jensen L, Åstrand P-O, Osted A, Kongsted J, Mikkelsen KV. Polarizability of molecular clusters as calculated by a dipole interaction model. J Chem Phys 2002;116(10):4001–10. http://dx.doi.org/10.1063/1.1433747.

[71] Applequist J, Sundberg KR, Olson ML, Weiss LC. A normal mode treatment of optical properties of a classical coupled dipole oscillator system with Lorentzian band shapes. J Chem Phys 1979;70(3):1240–6. http://dx.doi.org/10.1063/1.437616.

[72] Shanker B, Applequist J. Electronic absorption spectra of molecules and aggregates with interatomic charge transfer using a normal mode treatment of the atomic monopole–dipole interaction model. J Chem Phys 1996;104(16):6109–16. http://dx.doi.org/10.1063/1.471651.

[73] Smalø HS, Åstrand P-O, Mayer A. Combined nonmetallic electronegativity equalisation and point–dipole interaction model for the frequency-dependent polarisability. Mol Phys 2013;111(9–11):1470–81. http://dx.doi.org/10.1080/00268976.2013.797116.

[74] Haghdani S, Davari N, Sandnes R, Åstrand P-O. Complex frequency-dependent polarizability through the $\pi \rightarrow \pi^*$ excitation energy of azobenzene molecules by a combined charge-transfer and point-dipole interaction model. J Phys Chem A 2014;118(47):11282–92. http://dx.doi.org/10.1021/jp507639z.

[75] Davari N, Haghdani S, Åstrand P-O, Schatz GC. Local electric field factors by a combined charge-transfer and point–dipole interaction model. RSC Adv 2015;5(40):31594–605. http://dx.doi.org/10.1039/C5RA04183J.

[76] Moulin F, Devel M, Picaud S. Optical properties of soot nanoparticles. J Quant Spectrosc Radiat Transfer 2008;109(10):1791–801. http://dx.doi.org/10.1016/j.jqsrt.2008.01.016.

[77] Langlet R, Vanacharla M, Picaud S, Devel M. Bottom-up multi-step approach to study the relations between the structure and the optical properties of carbon soot nanoparticles. J Quant Spectrosc Radiat Transfer 2009;110(14–16):1615–27. http://dx.doi.org/10.1016/j.jqsrt.2009.03.015.

[78] García Fernández C, Picaud S, Devel M. Calculations of the mass absorption cross sections for carbonaceous nanoparticles modeling soot. J Quant Spectrosc Radiat Transfer 2015;164:69–81. http://dx.doi.org/10.1016/j.jqsrt.2015.05.011.

[79] Rérat M, Rayez J-C, Fábián B, Devel M, Picaud S. A CRYSTAL-based parameterization of carbon atom dynamic polarizabilities to compute optical properties of curved carbonaceous nanostructures. Theor Chem Acc 2022;141(11):65. http://dx.doi.org/10.1007/s00214-022-02926-1.

[80] Baldelli A, Trivanovic U, Rogak SN. Electron tomography of soot for validation of 2D image processing and observation of new structural features. Aerosol Sci Technol 2019;53(5):575–82. http://dx.doi.org/10.1080/02786826.2019.1578860.

[81] Baldelli A, Trivanovic U, Sipkens TA, Rogak SN. On determining soot maturity: A review of the role of microscopy-and spectroscopy-based techniques. Chemosphere 2020;252:126532. http://dx.doi.org/10.1016/j.chemosphere.2020.126532.

[82] Pascazio L, Martin JW, Bowal K, Akroyd J, Kraft M. Exploring the internal structure of soot particles using nanoindentation: A reactive molecular dynamics study. Combust Flame 2020;219:45–56. http://dx.doi.org/10.1016/j.combustflame.2020.04.029.

[83] Jacobson RS, Korte AR, Vertes A, Miller JH. The molecular composition of soot. Angew Chem 2020;132(11):4514–20. http://dx.doi.org/10.1002/ange.201914115.

[84] Veronesi S, Commodo M, Basta L, De Falco G, Minutolo P, Kateris N, Wang H, D'Anna A, Heun S. Morphology and electronic properties of incipient soot by scanning tunneling microscopy and spectroscopy. Combust Flame 2022;243:111980. http://dx.doi.org/10.1016/j.combustflame.2021.111980.

[85] Russo C, Apicella B, Ciajolo A. Hydrogen, sp^2 carbon hybridization, and sp^2 clustering as pieces of the puzzling nanostructure of soot: A closer look. Energy Fuels 2023;37(17):12525–40. http://dx.doi.org/10.1021/acs.energyfuels.3c01194.

[86] Marques MA, Gross EK. Time-dependent density functional theory. In: A primer in density functional theory. Springer; 2003, p. 144–84.

[87] Draine BT, Lee HM. Optical properties of interstellar graphite and silicate grains. Astrophys J 1984;285:89–108. http://dx.doi.org/10.1086/162480.

[88] Laor A, Draine BT. Spectroscopic constraints on the properties of dust in active galactic nuclei. Astrophys J 1993;402:441–68. http://dx.doi.org/10.1086/172149.

[89] Draine B. Scattering by interstellar dust grains. II. X-rays. Astrophys J 2003;598(2):1026. http://dx.doi.org/10.1086/379123.

[90] Senet P, Henrard L, Lambin P, Lucas A, Kuzmany H, Fink J, Mehring M, Roth S. A one parameter model of the UV spectra of carbon. In: Proceedings of the international winterschool on electronic properties of novel materials. Progress in fullerene research. World Scientific; 1994, p. 393–6.

[91] Marques MA, Castro A, Bertsch GF, Rubio A. Octopus: A first-principles tool for excited electron–ion dynamics. Comput Phys Comm 2003;151(1):60–78. http://dx.doi.org/10.1016/S0010-4655(02)00686-0.

[92] Castro A, Appel H, Oliveira M, Rozzi CA, Andrade X, Lorenzen F, Marques MA, Gross E, Rubio A. Octopus: A tool for the application of time-dependent density functional theory. Phys Status Solidi b 2006;243(11):2465–88. http://dx.doi.org/10.1002/pssb.200642067.

[93] Yabana K, Nakatsukasa T, Iwata J-I, Bertsch G. Real-time, real-space implementation of the linear response time-dependent density-functional theory. Phys Status Solidi b 2006;243(5):1121–38. http://dx.doi.org/10.1002/pssb.200642005.

[94] Sternheimer R. On nuclear quadrupole moments. Phys Rev 1951;84:244–53. http://dx.doi.org/10.1103/PhysRev.84.244.

[95] Malloci G, Mulas G, Joblin C. Electronic absorption spectra of PAHs up to vacuum UV-towards a detailed model of interstellar PAH photophysics. Astron Astrophys 2004;426(1):105–17. http://dx.doi.org/10.1051/0004-6361:20040541.

[96] Malloci G, Joblin C, Mulas G. On-line database of the spectral properties of polycyclic aromatic hydrocarbons. Chem Phys 2007;332(2–3):353–9. http://dx.doi.org/10.1016/j.chemphys.2007.01.001.

[97] Malloci G, Cappellini G, Mulas G, Mattoni A. Electronic and optical properties of families of polycyclic aromatic hydrocarbons: A systematic (time-dependent) density functional theory study. Chem Phys 2011;384(1–3):19–27. http://dx.doi.org/10.1016/j.chemphys.2011.04.013.

[98] Straatsma T, Philippopoulos M, McCammon J. NWChem: Exploiting parallelism in molecular simulations. Comput Phys Comm 2000;128(1–2):377–85. http://dx.doi.org/10.1016/S0010-4655(00)00054-0.

[99] Windus TL, Bylaska EJ, Dupuis M, Hirata S, Pollack L, Smith DM, Straatsma TP, Aprà E. NWChem: New functionality. In: Computational science—ICCS 2003: international conference, melbourne, Australia and St. Petersburg, Russia, June 2–4, 2003 proceedings, part IV 3. Springer; 2003, p. 168–77.

[100] Langhoff SR. Theoretical infrared spectra for polycyclic aromatic hydrocarbon neutrals, cations, and anions. J Phys Chem 1996;100(8):2819–41. http://dx.doi.org/10.1021/jp952074g.

[101] Bauschlicher CW, Langhoff SR. The calculation of accurate harmonic frequencies of large molecules: the polycyclic aromatic hydrocarbons, a case study. Spectrochim Acta A 1997;53(8):1225–40. http://dx.doi.org/10.1016/S1386-1425(97)00022-X.

[102] Hudgins DM, Bauschlicher Jr. CW, Allamandola LJ. Closed-shell polycyclic aromatic hydrocarbon cations: a new category of interstellar polycyclic aromatic hydrocarbons. Spectrochim Acta A 2001;57(4):907–30. http://dx.doi.org/10.1016/S1386-1425(00)00453-4.

[103] Becke A. Density-functional thermochemistry. III. The role of exact exchange. J Chem Phys 1993;98:5648–52. http://dx.doi.org/10.1063/1.464913.

[104] Stephens PJ, Devlin FJ, Chabalowski CF, Frisch MJ. Ab initio calculation of vibrational absorption and circular dichroism spectra using density functional force fields. J Phys Chem 1994;98(45):11623–7.

[105] Frisch MJ, Pople JA, Binkley JS. Self-consistent molecular orbital methods 25. Supplementary functions for Gaussian basis sets. J Chem Phys 1984;80(7):3265–9. http://dx.doi.org/10.1063/1.447079.

[106] Johnson III RD. NIST computational chemistry comparison and benchmark database. NIST Standard Reference Database Number 101 Release 22, 2022, May 2022. https://cccbdb.nist.gov.

[107] Perdew JP, Ernzerhof M, Burke K. Rationale for mixing exact exchange with density functional approximations. J Chem Phys 1996;105(22):9982–5. http://dx.doi.org/10.1063/1.472933.

[108] Castro A, Marques MA, Rubio A. Propagators for the time-dependent Kohn–Sham equations. J Chem Phys 2004;121(8):3425–33. http://dx.doi.org/10.1063/1.1774980.

[109] Gomez Pueyo A, Marques MA, Rubio A, Castro A. Propagators for the time-dependent Kohn–Sham equations: Multistep, Runge–Kutta, exponential Runge–Kutta, and commutator free Magnus methods. J Chem Theory Comput 2018;14(6):3040–52. http://dx.doi.org/10.1021/acs.jctc.8b00197.

[110] Jäger C, Henning T, Schlögl R, Spillecke O. Spectral properties of carbon black. J Non-Cryst Solids 1999;258(1–3):161–79.

[111] Mennella V, Colangeli L, Bussoletti E, Palumbo P, Rotundi A. A new approach to the puzzle of the ultraviolet interstellar extinction bump. Astrophys J 1998;507(2):L177.